

Cite this: *Mater. Adv.*, 2024,  
5, 3794

# Interactions between alkali cations and cyanide-bridged network in $A_2Co_4[Fe(CN)_6]_{3.3}$ Prussian blue analogues revealed by far-infrared spectroscopy†

 Maria Dronova,<sup>ab</sup> Laura Altmenschmidt,<sup>ab</sup> Amélie Bordage,<sup>ib</sup> Jean-Blaise Brubach,<sup>b</sup> Marine Verseils,<sup>b</sup> Gregory Balthazar,<sup>a</sup> Pascale Roy<sup>b</sup> and Anne Bleuzen<sup>ib</sup>\*<sup>a</sup>

A series of Prussian Blue Analogues (PBAs) having the chemical formula  $A_2Co_4[Fe(CN)_6]_{3.3} \cdot nH_2O$  ( $A^+ = Na^+, Rb^+$  and  $Cs^+$ ) was investigated by variable temperature far-infrared spectroscopy. Despite the same chemical composition of the cyanide-bridged CoFe network, the three compounds are known to exhibit different switching properties assignable to different interactions between the alkali cations and the cyanide-bridged CoFe network. **Na<sub>2</sub>CoFe** exhibits the thermally activated  $Co^{II}(\text{High Spin})Fe^{III} \rightarrow Co^{III}(\text{Low Spin})Fe^{II}$  electron transfer upon cooling, whereas **Rb<sub>2</sub>CoFe** and **Cs<sub>2</sub>CoFe** are already in the  $Co^{III}(\text{Low Spin})Fe^{II}$  electronic state at room temperature and remain in this electronic state upon cooling. Our variable temperature far-infrared spectroscopy study shows that the bands corresponding to the vibrations of the cyanide-bridged CoFe network and to the alkali cations exhibit different thermal behaviors upon cooling in the three compounds. These differences can be related to different interactions between the alkali cations and the cyanide-bridged CoFe network. Thus, far Infrared spectroscopy turns out to be a valuable tool to study these interactions so difficult to experimentally probe but which nevertheless play a crucial role in the properties of the compounds.

Received 22nd January 2024,  
Accepted 15th March 2024

DOI: 10.1039/d4ma00064a

rsc.li/materials-advances

## Introduction

Thanks to their versatile chemistry and the disorder inherent in their crystallographic structure, Prussian Blue Analogues (PBAs) exhibit a wide range of properties (magnetism,<sup>1</sup> electronic switching,<sup>2</sup> cations intercalation,<sup>3</sup> redox,<sup>4</sup> . . .) interesting for various applications (memory devices,<sup>2</sup> sensors,<sup>3</sup> batteries,<sup>4</sup> catalysis,<sup>5</sup> . . .). PBAs form a class of coordination polymers of chemical formula  $A_xM_p[M'(CN)_6]_q \cdot nOH_2$ , where  $M^{2+/3+}$  and  $M'^{2+/3+}$  are transition metal ions,  $A^+$  is a cation belonging most often to the first group of the periodic table of elements and □

is a  $M'(CN)_6$  vacancy. Their structure is complex,<sup>6</sup> but it can often be described in terms of the cubic structure with a face-centered lattice.<sup>7–9</sup> The  $M^{2+/3+}$  and  $M'^{2+/3+}$  transition metal ions, bridged by  $CN^-$  anions, form a bimetallic network made of strong chemical bonds; in the vicinity of the  $M'(CN)_6$  vacancies, the  $M^{2+/3+}$  ions complete their coordination sphere with water molecules. The  $A^+$  cations occupy various interstitial sites and some other zeolitic water molecules fill the remaining cavities. A scheme of one unit cell of the compounds of chemical formula  $A_2Co_4[Fe(CN)_6]_{3.3} \cdot nOH_2$ , which are investigated in the following, is displayed in Fig. 1. The structure of most PBAs exhibits a certain degree of intrinsic disorder due to the presence of a variable amount of  $M'(CN)_6$  vacancies, a variable amount of interstitial cations in ill-defined sites, and a variable amount of water molecules (either zeolitic or linked to the  $M^{2+/3+}$  cation), as well as possible distortion or tilting of the transition metal ion coordination spheres.<sup>10</sup> Except for some particular compounds generally containing many interstitial cations and few vacancies,<sup>11,12</sup> these defects do not exhibit long range order, so that their local effect on the structure and consequently on the properties of the compounds is extremely difficult to assess.

Infrared spectroscopy, sensitive to the vibration of all species present in the PBAs, is a possible tool to get valuable

<sup>a</sup> Institut de chimie moléculaire et des matériaux d'Orsay (ICMMO), Université Paris-Saclay, CNRS, 17 avenue des Science, 91400 Orsay, France.

E-mail: anne.bleuzen@universite-paris-saclay.fr

<sup>b</sup> Synchrotron SOLEIL, L'Orme des Merisiers Saint-Aubin, BP 48, 91192 Gif-sur-Yvette, France

† Electronic supplementary information (ESI) available: FIR spectra of CoFe PBAs of chemical formula  $Cs_xCo_4[Fe(CN)_6]_{(8+x)/3} \cdot nH_2O$  at 300 K; FIR spectra of **Na<sub>2</sub>CoFe**, **Rb<sub>2</sub>CoFe** and **Cs<sub>2</sub>CoFe** recorded upon cooling; FIR spectra of **Rb<sub>2</sub>CoFe** at 300 K before cooling and after 1 and 2 cooling/heating cycles; low temperature XANES spectra of **Na<sub>2</sub>CoFe**, **Rb<sub>2</sub>CoFe** and **Cs<sub>2</sub>CoFe** at the Co and Fe K-edges; MIR spectra of **Na<sub>2</sub>CoFe**, **Rb<sub>2</sub>CoFe** and **Cs<sub>2</sub>CoFe** over the 3400–3800  $cm^{-1}$  frequency range; frequency of absorbance maximum, full-width at half maximum and area under peak for the three Gaussian components ( $G_1$ ,  $G_2$ ,  $G_3$ ). See DOI: <https://doi.org/10.1039/d4ma00064a>





Fig. 1 Scheme of one unit cell of the  $A_2Co_4[Fe(CN)_6]_{3.3}\square_{0.7}\cdot nOH_2$  PBAs (brown balls stand for alkali cations, blue for Co ions, yellow for Fe ions, light grey for carbon atoms, dark grey for nitrogen atoms, and red for oxygen atoms). Zeolitic water molecules are omitted for clarity.

information on these defects and their role in the properties. Nevertheless, the study of PBAs by infrared spectroscopy has been so far most often restricted to the Middle-Infra-Red (MIR) range, where the cyanide ion vibration bands give information on the bridging character of the cyanide ion and the oxidation states of the transition metal ions.<sup>13–16</sup> In this MIR range, dynamical studies were also performed to monitor the charge transfer in the  $RbMn[Fe(CN)_6]$  PBA for instance.<sup>17–19</sup> Some studies then extended the investigation of PBA in the Far-InfraRed (FIR) range, where, in addition to the M–NC and M'–CN bonds,<sup>20,21</sup> the vibrations of the alkali cation is accessible.<sup>22</sup> The development of computational capacities also opened the door towards a theoretical support to assign the experimental bands in the whole (MIR and FIR) spectrum and so to push forward our microscopic knowledge of PBAs.<sup>21,22</sup> In this work, a series of three powdered CoFe PBAs of chemical formula  $A_2Co_4[Fe(CN)_6]_{3.3}\square_{0.7}\cdot nOH_2$  ( $A^+ = Cs^+, Rb^+$  and  $Na^+$ ) was investigated by variable temperature synchrotron FIR spectroscopy. They are called  $Na_2CoFe$ ,  $Rb_2CoFe$ , and  $Cs_2CoFe$  in the following. The stoichiometry of the cyanide-bridged CoFe network is exactly the same in the three compounds, only the nature of the alkali cations in the interstitial sites and the amount of zeolitic water molecules vary from one compound to another. Their thermal behaviors have already been reported.<sup>23–25</sup>  $Na_2CoFe$  exhibits the thermally activated  $Co^{II}(High\ Spin)Fe^{III} \rightarrow Co^{III}(Low\ Spin)Fe^{II}$  electron transfer upon cooling, whereas  $Rb_2CoFe$  and  $Cs_2CoFe$  show no such change and remain in the  $Co^{III}(low\ spin)Fe^{II}$  electronic state within the whole temperature range. These different behaviors arise from the different nature of the alkali cation, which differently interacts with the cyanide-bridged CoFe network in the three compounds. Nevertheless, direct and unambiguous information on these interactions is still missing. Hence, as a probe of all chemical bonds, *in situ* FIR spectroscopy has been used here as an original tool to investigate these interactions between the alkali cations and the cyanide-bridged bimetallic network.

## Results and discussion

### Attribution of the bands

The room temperature FIR spectra for the  $A_2CoFe$  series are displayed in Fig. 2, where the spectrum of  $Na_2CoFe$  is also compared to the one recorded at 14 K.

First of all, one can observe from the spectra at 300 K that the series can be splitted into two groups:  $Rb_2CoFe$  and  $Cs_2CoFe$  on the one side, with a very similar spectral shape, and on the other side  $Na_2CoFe$ , which displays a very different spectrum at room temperature.

$Na_2CoFe$  is known to display a thermally activated electronic switching previously investigated by SQUID magnetometry<sup>23</sup> and  $L_{2,3}$ -edge X-ray absorption spectroscopy.<sup>24</sup> The results from these studies show that  $Na_2CoFe$  is found to be in the  $Co^{II}(HS)-Fe^{III}$  state at room temperature and in the  $Co^{III}(LS)Fe^{II}$  states at 14 K.<sup>23,24</sup> The same conclusions have been reached by Lejeune and co-workers<sup>20,26</sup> from the FIR spectra of  $Na_2CoFe$  at the corresponding temperatures. Thanks to (i) the comparison of the spectra at 300 K and 14 K, and (ii) the presence of bands situated at comparable frequencies on the spectra of the  $[M(NH_3)_6]^{k+}$  and  $[M(CN)_6]^{j-}$  complexes,<sup>27,28</sup> the bands in the 200–300  $cm^{-1}$  and the 400–600  $cm^{-1}$  regions were attributed to vibration modes of the cyanide-bridged CoFe network and associated, respectively, with the Co–NC and Fe–CN bonds.<sup>20</sup> We remind here the main conclusions. At room temperature, *i.e.* in the  $Co^{II}Fe^{III}$  state, the band at 220  $cm^{-1}$  corresponds to the  $Co^{II}$ –NC bonds and the one at 433  $cm^{-1}$  to the  $Fe^{III}$ –CN bonds. Upon cooling, the intensity of these two bands decreases, with a concomitant increase of two bands at

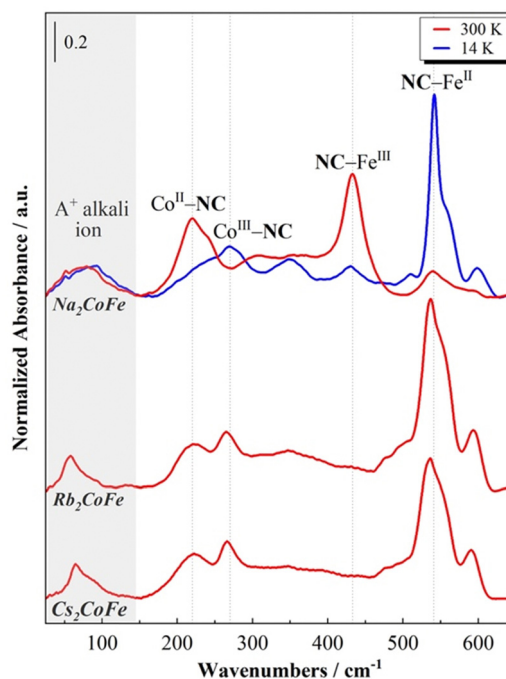


Fig. 2 Far-Infrared spectra of the  $A_2CoFe$  PBAs at 300 K and of  $Na_2CoFe$  at 14 K. The spectra were normalized by the NC–Fe band maximum of their  $Co^{III}Fe^{II}$  state at 14 K.

270  $\text{cm}^{-1}$  and 542  $\text{cm}^{-1}$ . Since the low temperature state of  $\text{Na}_2\text{CoFe}$  is known to be  $\text{Co}^{\text{III}}\text{Fe}^{\text{II}}$ , they were respectively attributed to the  $\text{Co}^{\text{III}}\text{-NC}$  and  $\text{Fe}^{\text{II}}\text{-CN}$  bonds. Comparable bands were observed on the FIR spectrum of the  $\text{Mn}^{\text{II}}\text{Fe}^{\text{III}}$  PBA with comparable structure and containing four  $\text{Cs}^+$  cations per unit cell (and no  $\text{Fe}(\text{CN})_6$  vacancy) in ref. 21; based on first-principles phonon mode calculations, they were assigned to bending modes of the  $\text{Mn}\text{-NC}\text{-Fe}$  linkages. For the sake of clarity, we will keep associating them with the  $\text{Co}\text{-NC}$  and  $\text{Fe}\text{-CN}$  bonds, which nevertheless correspond to the main oscillators involved in each vibration mode.<sup>21</sup>

The FIR spectra of  $\text{Rb}_2\text{CoFe}$  and  $\text{Cs}_2\text{CoFe}$  at room temperature both display very similar spectral shape. They resemble the one of  $\text{Na}_2\text{CoFe}$  at low temperature, which is fully consistent with their  $\text{Co}^{\text{III}}\text{-Fe}^{\text{II}}$  ground state.<sup>24,25,29</sup> The main band around 540  $\text{cm}^{-1}$  is thus associated with the  $\text{Fe}^{\text{II}}\text{-CN}$  bonds and the one around 270  $\text{cm}^{-1}$  with the  $\text{Co}^{\text{III}}\text{-NC}$  bonds. The additional band around 215  $\text{cm}^{-1}$  is attributed to the  $\text{Co}^{\text{II}}\text{-NC}$  bonds, in agreement (i) with the spectrum of  $\text{Na}_2\text{CoFe}$  at room temperature and (ii) with the known presence of a small amount of  $\text{Co}^{2+}$  ions in  $\text{Rb}_2\text{CoFe}$  and  $\text{Cs}_2\text{CoFe}$ .<sup>25,29</sup>

In addition to these main bands, two additional bands can be observed around 600  $\text{cm}^{-1}$  and below 100  $\text{cm}^{-1}$ .

The band at 600  $\text{cm}^{-1}$  is not unambiguously attributed in the literature. Bands at similar frequencies have already been reported in some alkali-containing ( $\text{Cs}^+$ ,  $\text{Na}^+$ ,  $\text{K}^+$ ) zinc ferrocyanides.<sup>30</sup> Here, it is observed in the  $\text{Co}^{\text{III}}\text{Fe}^{\text{II}}$  state (*i.e.* at 300 K for  $\text{Rb}_2\text{CoFe}$  and  $\text{Cs}_2\text{CoFe}$ , and at 14 K for  $\text{Na}_2\text{CoFe}$ ), but it is nearly absent on the spectrum of  $\text{Na}_2\text{CoFe}$  at room temperature. Thus, it could be attributed to either a vibration mode of or specific  $\text{Fe}^{\text{II}}\text{-CN}$  bonds. However, bands around this frequency are also observed for  $\text{Co}\text{-O}$  bonds in  $\text{Co}$  oxides, in  $\text{Co}$  oxy-hydroxides and in transition metal based MOFs.<sup>31,32</sup> This band could therefore also be related to the presence of deprotonated  $\text{Co}^{\text{III}}\text{-O}$  bonds. The assignment of this band will be further discussed in the following.

Below 100  $\text{cm}^{-1}$ , an additional band is observed, located at different frequencies for the three PBAs, whatever the temperature and so the electronic state of the  $\text{Co}$  and  $\text{Fe}$  ions (Fig. 2). We propose to attribute this band to the vibration mode of the alkali cation ( $\text{Na}^+$ ,  $\text{Rb}^+$  or  $\text{Cs}^+$ ) in interstitial sites of the PBA, in agreement with the theoretical and experimental study by Ohkoshi and co-workers of the  $\text{Cs}^+$  vibration mode in the  $\text{Cs}_{0.9}\text{Mn}[\text{Fe}(\text{CN})_6]_{0.93}$  PBA.<sup>22</sup> One can see that the shape of this contribution varies along the series. On the spectrum of  $\text{Cs}_2\text{CoFe}$  at room temperature, it is comprised of a narrow peak at 65  $\text{cm}^{-1}$  and a broad shoulder around 80  $\text{cm}^{-1}$ . In a series of  $\text{CoFe}$  PBAs, containing a decreasing amount of  $\text{Fe}(\text{CN})_6$  vacancies and an increasing amount of  $\text{Cs}^+$  cations (Fig. S1, ESI<sup>†</sup>), the broad contribution disappears for the compound containing the minimum  $\text{Fe}(\text{CN})_6$  vacancies, whereas the narrow peak vanishes for the compound containing more than one  $\text{Fe}(\text{CN})_6$  vacancy per  $\text{Cs}^+$  ion (the unit cell of  $\text{Cs}_{0.7}$  contains 0.7  $\text{Cs}^+$  cation and 1.1  $\text{Fe}(\text{CN})_6$  vacancies). Thus, we propose to assign the narrow peak to the vibration of the  $\text{Cs}^+$  ion in the closed cubic  $\text{Co}_4\text{Fe}_4$  cavity (Fig. 3a) and the broad component to its vibration in an open  $\text{Co}(\text{Co}(\text{OH}_2))_3\text{Fe}_3$  (Fig. 3b) (or  $(\text{Co}(\text{OH}_2))_2(\text{Co}(\text{OH}_2)_2)_2\text{Fe}_2$ ) cavity.



Fig. 3 Scheme of (a) the closed and (b) the open  $\text{Co}(\text{Co}(\text{OH}_2))_3\text{Fe}_3$  Cavities and the proposed positioning for the bigger alkali cations ( $\text{Rb}^+$ ,  $\text{Cs}^+$ ) in each of them.

As the size of the  $\text{Cs}^+$  cation matches the size of the closed cavity, this ion interacts with several surrounding cyanide bridging ions and its environment is well-defined, leading to a narrow peak. In contrast, for an open cavity, a wider range of environments can accommodate the  $\text{Cs}^+$  ions that are even likely to move from one to the other, resulting in a broader band. Thus, this suggests that the width of the contribution reflects the cation-to-cavity volumic ratio and an explanation for the variable shape of this band can be proposed along the  $\text{A}_2\text{CoFe}$  series. The shape of the spectra of  $\text{Rb}_2\text{CoFe}$  and  $\text{Cs}_2\text{CoFe}$  below 100  $\text{cm}^{-1}$  is comparable because the size of the  $\text{Rb}^+$  and the  $\text{Cs}^+$  ion is close. Like for the  $\text{Cs}^+$  ion, the narrow peak is assignable to  $\text{Rb}^+$  ions in the closed cubic  $\text{Co}_4\text{Fe}_4$  cavities (Fig. 3a) and the broader contribution to  $\text{Rb}^+$  ions in open  $\text{Co}(\text{Co}(\text{OH}_2))_3\text{Fe}_3$  (Fig. 3b) (or  $(\text{Co}(\text{OH}_2))_2(\text{Co}(\text{OH}_2)_2)_2\text{Fe}_2$ ) cavities. In contrast, the  $\text{Na}^+$  ion is significantly smaller than the two others, so that, whatever the closed or open cavity it is located in, the cation-to-cavity volumic ratio is always low, leading to a wider range of possible environments for the  $\text{Na}^+$  cation whatever the kind of cavity. This wider range of environments can explain the broadness of the band for the same amount of  $\text{Fe}(\text{CN})_6$  vacancies as in the two other compounds.

At last, it is noticeable that the shape of the alkali cation vibration band, which we just related to the nature of the alkali cation and its environment, seems also to be connected to the electronic state of the compound at room temperature. Thus, the same broad band is observed on the spectra of  $\text{Na}_2\text{CoFe}$  and  $\text{Cs}_{0.7}\text{CoFe}$  (Fig. 2 and Fig. S1, ESI<sup>†</sup>), which are both stabilized in the  $\text{Co}^{\text{II}}\text{Fe}^{\text{III}}$  electronic state at 300 K.<sup>20,23,25</sup> In contrast, a peak, with a shoulder on the high frequencies side, is observed on the spectra of  $\text{Cs}_2\text{CoFe}$  and  $\text{Rb}_2\text{CoFe}$  (Fig. 2), which are both in the  $\text{Co}^{\text{III}}\text{Fe}^{\text{II}}$  electronic state at room temperature. In the latter, the  $\text{Co}^{\text{III}}\text{Fe}^{\text{II}}$  electronic state is formed through a redox reaction in solution during the synthesis of the compounds. The relationship between the electronic state of the compound and the shape of the alkali cation vibration band suggests that the presence of big alkali cations in closed cubic cavities (associated with the narrow peak on the spectra) plays a key role in the  $\text{Co}^{\text{II}}\text{Fe}^{\text{III}} \rightarrow \text{Co}^{\text{III}}\text{Fe}^{\text{II}}$  redox reaction accompanying the formation of the compound.

The complete list of assigned frequencies is given in Table 1.

### Effect of the temperature on the spectra

The spectra of  $\text{Na}_2\text{CoFe}$ ,  $\text{Rb}_2\text{CoFe}$  and  $\text{Cs}_2\text{CoFe}$  recorded upon cooling are shown in Fig. S2 (ESI<sup>†</sup>). For all compounds the



Table 1 Frequencies and bands assignment in  $\text{cm}^{-1}$  at 300 K and 14 K

|                                    | $\text{Na}_2\text{CoFe}$ |       | $\text{Rb}_2\text{CoFe}$ |       | $\text{Cs}_2\text{CoFe}$ |       |
|------------------------------------|--------------------------|-------|--------------------------|-------|--------------------------|-------|
|                                    | 300 K                    | 14 K  | 300 K                    | 14 K  | 300 K                    | 14 K  |
| $\text{Co}^{\text{II}}\text{-NC}$  | 219.8                    | —     | 221.3                    | 223.9 | 222.3                    | 220.1 |
| $\text{Co}^{\text{III}}\text{-NC}$ | —                        | 269.5 | 264.9                    | 270   | 266.1                    | 271.4 |
| $\text{Fe}^{\text{III}}\text{-CN}$ | 432.7                    | —     | —                        | —     | —                        | —     |
| $\text{Fe}^{\text{II}}\text{-CN}$  | —                        | 541.7 | 536.6                    | 540   | 536.4                    | 540.5 |
| $\text{A}^+$                       | 79.8                     | 92.8  | 58.3                     | 53.3  | 64.6                     | 63.6  |
| <sup>a</sup>                       | —                        | 598.5 | 593.2                    | 600.7 | 590.6                    | 599.3 |

<sup>a</sup> Possible attribution discussed in the text.

spectra at 300 K and at 14 K are different, but these changes are fully reversible, as shown on the spectrum of  $\text{Rb}_2\text{CoFe}$  at 300 K before cooling and after two cooling/heating cycles (Fig. S3, ESI†). The samples can be classified into the same two groups.

The spectral changes for  $\text{Na}_2\text{CoFe}$  (Fig. 2) are dominated by the thermally activated  $\text{Co}^{\text{II}}(\text{HS})\text{Fe}^{\text{III}} \rightarrow \text{Co}^{\text{III}}(\text{LS})\text{Fe}^{\text{II}}$  electronic switching as stated in the above discussion. They reflect an abrupt electronic switching (Fig. S2, ESI†) in agreement with magnetic measurements.<sup>23</sup> The weak intensity of the  $\text{Fe}^{\text{III}}\text{-CN}$  band ( $430 \text{ cm}^{-1}$ ) at low temperature indicates that the  $\text{Co}^{\text{II}}(\text{HS})\text{-Fe}^{\text{III}} \rightarrow \text{Co}^{\text{III}}(\text{LS})\text{Fe}^{\text{II}}$  electron transfer upon cooling is almost total. At last, the broad contribution at  $80 \text{ cm}^{-1}$  assigned to the vibration of the  $\text{Na}^+$  cation remains broad upon cooling (Fig. 4a). This can again be explained by the small size of the cation and the associated multiple positions of the latter in the cavities of the bimetallic network. Nevertheless, this contribution exhibits a significant change after the electron transfer, especially an upshift of the maximum of the band ( $+15 \text{ cm}^{-1}$ , *i.e.*  $+19\%$ ), showing that the electronic state change is accompanied with an important change in the vibrational properties of the  $\text{Na}^+$  cation.

$\text{Rb}_2\text{CoFe}$  and  $\text{Cs}_2\text{CoFe}$  are in the  $\text{Co}^{\text{III}}(\text{LS})\text{Fe}^{\text{II}}$  electronic state over the whole temperature range. Their spectra are both dominated by thermal effects. The bands assigned to the vibrations of

the cyanide-bridged CoFe network exhibit a shift towards higher frequencies upon cooling:  $\text{Fe}^{\text{II}}\text{-CN}$  ( $+3\text{--}4 \text{ cm}^{-1}$ ),  $\text{Co}^{\text{III}}\text{-NC}$  ( $+5 \text{ cm}^{-1}$ ) (Fig. S2 and Table S1, ESI†). These high-frequency shifts can be assigned to lattice contraction effects usually observed upon cooling.

A closer look at the bands associated with the  $\text{Fe}^{\text{II}}\text{-CN}$  bonds ( $\approx 540 \text{ cm}^{-1}$ ) and with the alkali cations ( $\approx 60 \text{ cm}^{-1}$ ) highlights however some differences between  $\text{Rb}_2\text{CoFe}$  and  $\text{Cs}_2\text{CoFe}$  (Fig. 4). These bands show considerably larger changes for  $\text{Rb}_2\text{CoFe}$  than for  $\text{Cs}_2\text{CoFe}$  upon cooling. The concomitant change of these two bands suggests coupled effects, reflecting the same phenomenon. Since these bands are both expected to be affected by the interactions between the alkali cations and the cyanide-bridged CoFe bimetallic network, such a correlation likely reflects a change in these interactions. Such interactions (and so their modifications) are rarely detected in PBAs, except when the amounts of alkali cations and  $\text{M}(\text{CN})_6$  vacancies are sufficiently large and small respectively, which allows for these interactions to spread in a cooperative way over the whole crystal. In that particular case, powder X-ray diffraction reveals a distortion of the cyanide-bridged bimetallic network due to the tilting of the transition metal ions octahedral coordination polyhedra possibly accompanied by a displacement of the alkali cation off the center of the cubic cavities.<sup>10</sup> This is reminiscent of structural distortions reported for perovskites, for which the driving force is considered to be the underbonding of small cations with the surrounding anions in the cubic cavities.<sup>33</sup> Our  $\text{A}_2\text{CoFe}$  compounds do not exhibit such collective distortions. Indeed, they all contain less alkali cations and more  $\text{Fe}(\text{CN})_6$  vacancies than the compounds exhibiting collective distortions. Nevertheless, the changes observed on the two bands associated to the  $\text{Fe}^{\text{II}}\text{-CN}$  bonds and to the alkali cations (Fig. 4) suggest that the changes in the interactions between the alkali cations and the cyanide-bridged bimetallic network can be probed by FIR spectroscopy. Due to the alkali cations dilution and their various environments in closed and open cavities, the effects of these interactions remain localized and probably of lesser magnitude than in compounds where they spread in a cooperative way. It has also to be noted that in the  $\text{Co}^{\text{III}}\text{Fe}^{\text{II}}$  electronic state, all the chemical bonds in the  $\text{Co}^{\text{III}}\text{-NC-Fe}^{\text{II}}$  linkages, including the  $\text{Co}^{\text{III}}(\text{LS})\text{-NC}$  bond, are very covalent and strong, which can hinder/weaken any distortion of the cyanide-bridged bimetallic network driven by alkali cation-network interactions. Noteworthy, the peak of the vibration band of the alkali cation shows a significant shift to lower frequencies by  $5 \text{ cm}^{-1}$  (7%)<sup>‡</sup> upon cooling for the  $\text{Rb}^+$  cation (Fig. 4a), but almost no shift for the  $\text{Cs}^+$  cation (1%). The usual thermal effects are fully excluded here, since in such case, the shift is towards higher frequencies, as observed for the bands associated to the  $\text{Fe-CN}$  and  $\text{Co-NC}$  bonds (see above).



Fig. 4 Spectra of the  $\text{A}_2\text{CoFe}$  PBAs at 300 K and at 14 K over (a) the  $25\text{--}130 \text{ cm}^{-1}$  and (b) the  $510\text{--}530 \text{ cm}^{-1}$  spectral ranges. The spectra were normalized by the  $\text{NC-Fe}$  band maximum of their  $\text{Co}^{\text{III}}\text{Fe}^{\text{II}}$  state at 14 K.

<sup>‡</sup> It is noteworthy that the  $5 \text{ cm}^{-1}$  shift of the  $\text{Rb}^+$  band from  $58.3 \text{ cm}^{-1}$  to  $53.3 \text{ cm}^{-1}$  is significant and corresponds to a band shift of 7%. For comparison, the  $\approx 40 \text{ cm}^{-1}$  shift of the cyanide band in the Middle InfraRed accompanying the  $\text{Co}^{\text{III}}\text{CNFe}^{\text{II}}$  to  $\text{Co}^{\text{II}}\text{CNFe}^{\text{III}}$  electron transfer corresponds to a band shift of only 1.7%.



These different behaviours of the alkali cations vibration band thus reflect different interactions between the alkali cation and the surrounding  $\text{Co}_4\text{Fe}_4$  cage and can be explained by the different size of the alkali cations. Thus, the larger  $\text{Cs}^+$  cation fits particularly well the cubic cavities and interacts equally with all 12 surrounding cyanido ligands over the whole temperature range without either significant structural change of the surrounding cage or displacement of the alkali cation; the band associated to its vibrations does almost not change upon cooling. This is consistent with the very rare observation of octahedral tilting in  $\text{Cs}^+$ -rich PBAs.<sup>10</sup> In contrast, the smaller  $\text{Rb}^+$  cation accommodates less well to all the cyanido ligands of the cubic cage. Interaction of the  $\text{Rb}^+$  cation with fewer cyanido ligands is thus likely to be favored upon cooling, which can explain the shift of the  $\text{Rb}^+$  vibration band. Such underbonding of the  $\text{Rb}^+$  cations in the cubic cavity is not surprising, since octahedral tilting revealing such situations, has already been reported in  $\text{Rb}^+$ -rich PBAs.<sup>10,34–37</sup> Furthermore, the frequency downshift of the band is consistent with the expected softening of the cation vibration band associated to the off-centering (or the early stages of the off-centering) of the alkali cation inside the closed cubic cavity, as observed in displacive-type ferroelectric materials.<sup>§38–40</sup> A scheme illustrating the proposed positioning of the  $\text{Rb}^+$  and  $\text{Cs}^+$  cations in the closed cubic cavities is shown in Fig. 5. It is noticeable that such off-centering of the  $\text{Rb}^+$  cation has been observed in molecular cubic cage mimicking the octant of  $\text{CoFe}$  PBAs.<sup>41</sup>

The effects of interactions between the alkali cations and the cyanide-bridged  $\text{CoFe}$  network are also detectable in the  $\text{Fe}^{\text{II}}-\text{CN}$  bond vibration frequency range on the spectra of  $\text{Rb}_2\text{CoFe}$  and  $\text{Cs}_2\text{CoFe}$  (Fig. 4b and Fig. 6). The band assigned to the  $\text{Fe}^{\text{II}}-\text{CN}$  bond is asymmetric and can be described as a pair of bands (a narrow peak and a high frequency broad shoulder). These two contributions either correspond to two different vibration modes (stretching and deformation for instance) or reflect the presence of two different environments for the  $\text{Fe}^{\text{II}}(\text{CN})_6$  entities in the compounds. As the chemical composition of the cyanide-bridged  $\text{CoFe}$  network and the oxidation state of the transition metal ions are exactly the same in both compounds, the differences between these two contributions can be assigned to different interactions between the  $\text{Fe}^{\text{II}}(\text{CN})_6$  entities and the alkali cations. At room temperature, the shape of this band is very similar for both  $\text{Rb}_2\text{CoFe}$  and  $\text{Cs}_2\text{CoFe}$ , indicating comparable environments of the  $\text{Fe}^{\text{II}}(\text{CN})_6$  entities in both compounds (Fig. 6a). It also suggests comparable

§ Generally, the softening of one mode toward low frequency with temperature is a well known “soft-mode” behavior particularly studied and identified in ferroelectric materials. Indeed, based on Landau theory of phase transitions, Cochran has demonstrated that if a crystal undergoes a second order phase transition and if this transition is of the displacive type (the low temperature equilibrium positions of atoms can be described as a displacement of the atoms from their high temperature equilibrium positions),<sup>39,40</sup> it always exists a phonon whose frequency goes to zero at the critical temperature, while the other phonons frequencies remain finite. This theory was confirmed by the observation of very strong mode softening in ferroelectric materials,<sup>38</sup> where the ferroelectric transition corresponds to the off-centering of the cation that is inside the oxygen octahedra cage.

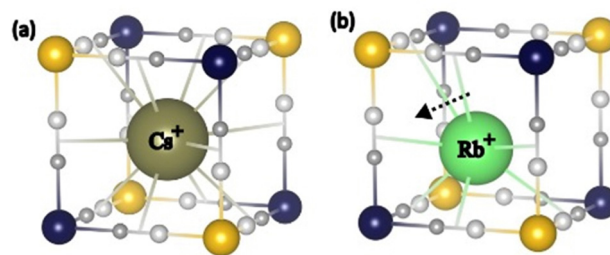


Fig. 5 Scheme of the proposed positioning of the (a)  $\text{Cs}^+$  and (b)  $\text{Rb}^+$  cations in the closed cubic cavities.



Fig. 6 Spectra of  $\text{Rb}_2\text{CoFe}$  and  $\text{Cs}_2\text{CoFe}$  over the 500–620  $\text{cm}^{-1}$  range at (a) 300 K and (b) at 14 K.

interactions between the alkali cations and the  $\text{Fe}^{\text{II}}(\text{CN})_6$  entities in both compounds. The shape of the  $\text{Fe}^{\text{II}}-\text{CN}$  band on the spectrum of  $\text{Cs}_2\text{CoFe}$  shows very little changes upon cooling (Fig. 4b), suggesting almost unchanged interactions between the  $\text{Cs}^+$  cation and the  $\text{Fe}^{\text{II}}(\text{CN})_6$  entities, in line with the unchanged vibration band of the  $\text{Cs}^+$  cation. The  $\text{Cs}^+$  cation fits perfectly well the cubic cage and interacts equally with the surrounding cyanido ligands whatever the temperature. In contrast, at low temperature, the relative intensity of the peak and shoulder of the band seems to be different between the two PBAs, with a significant evolution for  $\text{Rb}_2\text{CoFe}$  with respect to room temperature. The change in the intensity ratio between the peak and the shoulder upon cooling on the spectrum of  $\text{Rb}_2\text{CoFe}$  suggests different interactions between the  $\text{Rb}^+$  cation and the  $\text{Fe}^{\text{II}}(\text{CN})_6$  entities at 300 K and 14 K, in line with the shift of the vibration band of the  $\text{Rb}^+$  cation and the proposed reduced coordination number of the latter upon cooling.



## Effect of the alkali cation chemical nature on the Fe<sup>II</sup>-CN band at low temperature

At 14 K, the oxidation states of the transition metal ions (Fig. S4, ESI†) and the chemical composition of the cyanide bridged CoFe network are the same for **Cs<sub>2</sub>CoFe**, **Rb<sub>2</sub>CoFe** and **Na<sub>2</sub>CoFe**. Nevertheless, the shape of the Fe<sup>II</sup>-CN band is clearly different on the spectra of the three compounds (Fig. 7). The main difference between the three compounds is the chemical nature of the alkali cation. The different shape of the FIR spectrum over the 500–550 cm<sup>-1</sup> frequency range can therefore be assigned to different interactions between the alkali cations and the Fe(CN)<sub>6</sub> entities. The relative intensity of the peak and of the shoulder of the Fe<sup>II</sup>-CN band as well as that of the band at 600 cm<sup>-1</sup> seems to vary along the series. Fig. 7 shows the deconvolution of these bands into three Gaussian components for the three compounds and their frequency of absorbance maximum, full-width at half maximum and area under peak are given in Table S1 (ESI†). The results of the deconvolution show that the G1 peak displays the strongest variation with the chemical nature of the alkali cation. Its area under the peak decreases and the frequency of its absorbance maximum and linewidth increase as the size of the alkali cation increases from Na<sup>+</sup> to Cs<sup>+</sup>. The G1 peak can be assigned either to Fe(CN)<sub>6</sub> entities directly interacting with the alkali cations or to a vibration mode of the Fe(CN)<sub>6</sub> entities affected by the presence

of the alkali cations. In contrast, the G2 and G3 peaks exhibit very close absorbance maxima and linewidths for the three compounds. They can be assigned either to Fe(CN)<sub>6</sub> entities without significant interaction with the alkali cations or to vibration modes of the Fe(CN)<sub>6</sub> entities, which are not affected by the presence of the alkali cations. The assignment of the G3 peak to deprotonated Co<sup>III</sup>-O bonds can be ruled out. Indeed, in this case, a change in the stretching vibration bands of the OH bonds of water molecules coordinated to the Co ions in the MIR range should have an impact on this band. On the contrary, the G3 peak is unchanged while the stretching vibration bands of the OH bonds of water molecules bound to the Co ions of **Cs<sub>2</sub>CoFe** and **Rb<sub>2</sub>CoFe** on the one hand and of **Na<sub>2</sub>CoFe** on the other hand are much different (Fig. S5, ESI†).

All these results enable to better understand the interactions between the alkali cation and the cyanide-bridged CoFe bimetallic network, and to emphasize the role of the alkali cation in the different compounds. In the **A<sub>2</sub>CoFe** series of compounds containing the same number of alkali cations and Fe(CN)<sub>6</sub> vacancies, and therefore exhibiting the same Co<sub>4</sub>[Fe(CN)<sub>6</sub>]<sub>3.3</sub> chemical composition of the cyanide-bridged bimetallic network, three different thermal behaviors are indeed observed depending on the nature and, consequently, on the size of the alkali cation. As stated above, the evolution of the spectrum of **Cs<sub>2</sub>CoFe**, which is in the Co<sup>III</sup>Fe<sup>II</sup> electronic state whatever the temperature, is dominated upon cooling by pure thermal effects. The big Cs<sup>+</sup> cation fits the PBA's cavities particularly well without modification in the Cs<sup>+</sup>-cyanide-bridged CoFe network interactions upon cooling (Fig. 4). **Rb<sub>2</sub>CoFe** is in the same electronic state as **Cs<sub>2</sub>CoFe** whatever the temperature. However, despite comparable spectra for the main bands between **Rb<sub>2</sub>CoFe** and **Cs<sub>2</sub>CoFe** at 300 K, the spectrum of **Rb<sub>2</sub>CoFe** exhibits more significant changes than that of **Cs<sub>2</sub>CoFe** upon cooling, revealing different alkali cations thermal behaviours. These different thermal behaviours are assignable to their different sizes, resulting in different bondings with the surrounding anions. Finally, the spectrum evolution of **Na<sub>2</sub>CoFe** upon cooling is dominated by the thermally activated electron transfer. Nevertheless, the change of the Na<sup>+</sup> vibration band reflects an effect of the electron transfer on the interactions between the alkali cation and the cyanide-bridged CoFe network.

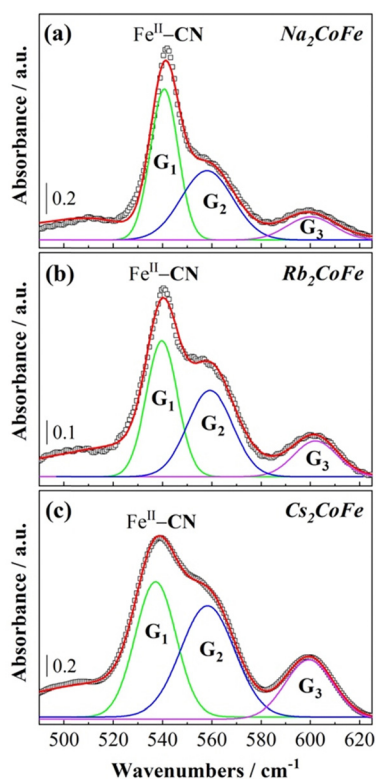


Fig. 7 Spectral deconvolution of (a) **Na<sub>2</sub>CoFe**, (b) **Rb<sub>2</sub>CoFe** and (c) **Cs<sub>2</sub>CoFe** over the 500–630 cm<sup>-1</sup> range at 14 K. The open squares represent the experimental points and the solid lines the Gaussian fitting curves.

## Experimental

### Compounds synthesis

The powdered CoFe Prussian Blue Analogues with chemical formula A<sub>2</sub>Co<sub>4</sub>[Fe(CN)<sub>6</sub>]<sub>3.3</sub>·nH<sub>2</sub>O (A= Na<sup>+</sup>, Rb<sup>+</sup> and Cs<sup>+</sup>) were prepared from a precipitation reaction in aqueous solutions of potassium ferricyanide(III) and cobalt(II) nitrate salts, by following the synthesis conditions as described in ref. 24. These samples are respectively called **Na<sub>2</sub>CoFe**, **Rb<sub>2</sub>CoFe** and **Cs<sub>2</sub>CoFe**. Their characterization using elemental analysis, X-ray diffraction, X-ray absorption spectroscopy and magnetization measurements can be found in a separate series of publications elsewhere.<sup>24,25,29,42,43</sup> The chemical composition, the



structure and the electronic state of the three compounds have been checked before recording the IR spectra.

### Infrared (IR) spectroscopy

The temperature-dependent far-infrared (FIR) spectroscopic studies were carried out on the beamline AILES at synchrotron SOLEIL (Gif sur Yvette, France).<sup>44</sup> Samples were prepared by dispersing the powders with Nujol oil to form a paste, which was placed in a liquid absorption cell between two diamond windows. All the measurements were acquired on a Bruker IFS 125 Fourier transform spectrometer equipped with a 6  $\mu\text{m}$  Si beam splitter and a 4.2 K liquid-helium-cooled Si bolometer detector to assess a far-IR spectral window ( $20 \leq \omega \leq 650 \text{ cm}^{-1}$ ). Prior to the measurements, the spectrometer was evacuated down to a  $2 \times 10^{-5}$  mbar pressure to minimize absorptions due to residual gases and to limit ice formation on the sample during the cooling down of the sample. The IR spectra were recorded upon cooling and heating cycles in the temperature range from 300 K to 14 K. The temperature on the sample was maintained using a temperature controller (Lake-shore model 336) connected to a thermostat, which is in thermal contact with a copper sample holder. All data were recorded in transmission mode. The reference spectrum was measured under the same conditions by using the sample holder filled with pure Nujol and then subtracted from all the subsequent data acquisition. Each spectrum was subjected to a linear baseline correction and removal of interference fringes arising from internal reflection within diamond windows.<sup>45</sup> Lastly, all spectra were normalized to a range [0, 1] by setting the maximum intensity value (of the Fe<sup>II</sup>-CN band at 14 K) at 1. The bands frequency determination were done by the use of the Origin software.

The uncertainty in bands position ( $\Delta\nu$ ) can be approximated as follows:  $\Delta\nu \approx \Delta W/2(S/N)$ , where  $\Delta W$  is the bandwidth at half-maximum and (S/N) represents the signal-to-noise ratio.<sup>46</sup> For the Rb<sup>+</sup> alkali cation band at  $53 \text{ cm}^{-1}$  (at 14 K), the width half-maximum of  $23.0 \text{ cm}^{-1}$  combined with the high signal-to-noise ratio of approximately 142 achieved using the synchrotron source, gives an accuracy for the band position better than  $0.08 \text{ cm}^{-1}$ . The peak maxima of other bands studied in detail, such as that of Fe-CN at  $540 \text{ cm}^{-1}$ , are defined with equivalent precision. Such precision fully validates the observed frequency shifts of a few wavenumbers.

## Conclusions

The use of far-infrared spectroscopy remains scarce in the investigation of the structure-properties relationships in Prussian blue analogues. This variable temperature study of the A<sub>2</sub>CoFe series demonstrates that FIR spectroscopy, despite the need of synchrotron radiation to be used, is particularly well-suited to probe the interactions between the alkali cations in interstitial sites of Prussian blue analogues and the surrounding cyanide-bridged bimetallic network. These interactions play a crucial role in the properties of the PBAs, but they can be

revealed only in favorable cases where they spread in a cooperative way in the compounds and can then be detected by powder XRD. Here, thanks to this proof-of-concept study, we show that FIR spectroscopy bring information in these interactions even for PBAs with few alkali cations and no cooperative effect. This paves the way towards a better understanding of the properties of PBAs where alkali cations play a key role.

## Conflicts of interest

There are no conflicts to declare.

## Acknowledgements

The authors acknowledge SOLEIL for the provision of synchrotron radiation facility on the AILES beamline through proposals 20201201 and 20220450. This work was supported by the Paris Ile-de-France region (DIM Respole). The authors thank K. Rader for technical support during experiments.

## Notes and references

- M. Verdager, A. Bleuzen, V. Marvaud, J. Vaisserman, M. Seuleiman, C. Desplanches, A. Sculler, C. Train, R. Garde, G. Gelly, C. Lomenech, I. Rosenman, P. Veillet and C. Cartier dit Moulin, *Coord. Chem. Rev.*, 1999, **190–192**, 1023.
- O. Sato, T. Iyoda, A. Fujishima and K. Hashimoto, *Science*, 1996, **272**, 704.
- J. Jang and D. S. Lee, *Ind. Eng. Chem. Res.*, 2016, **55**, 3852.
- Y. Lu, L. Wang, J. G. Cheng and J. B. Goodenough, *Chem. Commun.*, 2012, **48**, 6544.
- K. Itaya, N. Shoji and I. Uchida, *J. Am. Chem. Soc.*, 2010, **20**, 5110.
- A. Simonov, T. De Baerdemaeker, H. L. B. Boström, M. L. Rios Gomez, H. J. Gray, D. Chernyshov, A. Bosak, H.-B. Bürgi and A. L. Goodwin, *Nature*, 2020, **578**, 256.
- A. Lüdi, H.-U. Güdel and M. Rüegg, *Inorg. Chem.*, 1970, **9**(10), 2224.
- H. J. Buser, D. Schwarzenbach, W. Fetter and A. Lüdi, *Inorg. Chem.*, 1977, **16**, 2704.
- A. Lüdi and H. U. Güdel, *Structure and Bonding*, Springer-Verlag, Berlin, Germany, 1973, pp. 1–21.
- H. L. B. Boström and W. R. Brant, *J. Mater. Chem. C*, 2022, **10**, 13690.
- X. Bie, K. Kubota, T. Hosaka, K. Chiharab and S. Komaba, *J. Mater. Chem. A*, 2017, **5**, 4325.
- J. Cattermull, K. Sada, K. Hurlbutt, S. J. Cassidy, M. Pasta and A. L. Goodwin, *Chem. Mater.*, 2022, **34**, 5000.
- J. D. Qiu, H.-Z. Peng, R.-P. Liang, J. Li and X.-H. Xia, *Langmuir*, 2007, **23**, 2133.
- R. O. Lezna, R. Romagnoli, N. R. de Tacconi and K. Rajeshwar, *J. Phys. Chem. B*, 2002, **106**, 3612.
- N. Shimamoto, S.-I. Ohkoshi, O. Sato and K. Hashimoto, *Inorg. Chem.*, 2002, **41**, 678.



- 16 A. C. Felts, M. J. Andrus, C. M. Averback, C. H. Li and D. R. Talham, *Polyhedron*, 2017, **133**, 404.
- 17 T. Suemoto, K. Ohki, R. Fukaya, M. Nakajima, H. Tokoro and S. Ohkoshi, *J. Lumin.*, 2009, **129**, 1775.
- 18 T. Suemoto, R. Fukaya, A. Asahara, M. Nakajima, H. Tokoro and S. Ohkoshi, *Phys. Status Solidi B*, 2011, **248**, 477.
- 19 A. Asahara, M. Nakajima, R. Fukaya, H. Tokoro, S.-I. Ohkoshi and T. Suemoto, *Phys. Status Solidi B*, 2011, **248**, 491.
- 20 J. Lejeune, J.-B. Brubach, P. Roy and A. Bleuzen, *C. R. Chim.*, 2014, **17**, 534.
- 21 H. Tokoro, A. Namai, M. Yoshikiyo, R. Fujiwara, K. Chiba and S. Ohkoshi, *Sci. Rep.*, 2018, **8**, 63.
- 22 S.-I. Ohkoshi, M. Yoshikiyo, A. Namai, K. Nakagawa, K. Chiba, R. Fujiwara and H. Tokoro, *Sci. Rep.*, 2017, **7**, 8088.
- 23 R. Le Bris, J.-D. Cafun, C. Mathonière, A. Bleuzen and J.-F. Létard, *New J. Chem.*, 2009, **33**, 1255.
- 24 J.-D. Cafun, G. Champion, M.-A. Arrio, C. Cartier dit Moulin and A. Bleuzen, *J. Am. Chem. Soc.*, 2010, **132**, 11552.
- 25 V. Escax, A. Bleuzen, C. Cartier dit Moulin, F. Villain, A. Goujon, F. Varret and M. Verdaguer, *J. Am. Chem. Soc.*, 2001, **123**, 12536.
- 26 J. Lejeune, J.-D. Cafun, G. Fornasieri, J. B. Brubach, G. Creff, P. Roy and A. Bleuzen, *Eur. J. Inorg. Chem.*, 2012, 3980.
- 27 H. J. Llewellyn, *Inorg. Chem.*, 1963, **2**, 777.
- 28 K. Nakamoto, *Infrared and Raman Spectra of Inorganic and Coordination Compounds*, John Wiley & Sons, Inc., Hoboken, New Jersey, 2008.
- 29 A. Bleuzen, C. Lomenech, V. Escax, F. Villain, F. Varret, C. Cartier dit Moulin and M. Verdaguer, *J. Am. Chem. Soc.*, 2000, **122**, 6648.
- 30 C. Loos-Neskovic, M. Fedoroff and E. Garnier, *Talanta*, 1989, **36**, 749.
- 31 C.-W. Tang, C.-B. Wang and S.-H. Chien, *Thermochim. Acta*, 2008, **473**, 68.
- 32 K. I. Hadjiivanov, D. A. Panayotov, M. Y. Mihaylov, E. Z. Ivanova, K. K. Chakarova, S. M. Andonova and N. L. Drenchev, *Chem. Rev.*, 2021, **121**, 1286.
- 33 P. M. Woodward, *Acta Crystallogr., Sect. B: Struct. Sci.*, 1997, **53**, 44.
- 34 J.-H. Her, P. W. Stephens, C. M. Kareis, J. G. Moore, K. S. Min, J.-W. Park, G. Bali, B. S. Kennon and J. S. Miller, *Inorg. Chem.*, 2010, **49**, 1524.
- 35 T. Matsuda, J. Kim and Y. Moritomo, *Dalton Trans.*, 2012, **41**, 7620.
- 36 Y. Moritomo, M. Hanawa, Y. Ohishi, K. Kato, M. Takata, A. Kuriki, E. Nishibori, M. Sakata, S. Ohkoshi, H. Tokoro and K. Hashimoto, *Phys. Rev. B: Condens. Matter Mater. Phys.*, 2003, **68**, 144106.
- 37 H. L. B. Bostrom and R. I. Smith, *Chem. Commun.*, 2019, **55**, 10230.
- 38 J. Petzelt, G. V. Kozlov and A. A. Volkov, *Ferroelectrics*, 2011, **73**, 101.
- 39 W. Cochran, *Adv. Phys.*, 1960, **9**, 387.
- 40 S. Aubry and R. Pick, *J. Phys.*, 1971, **32**, 657.
- 41 J. Glatz, J.-R. Jiménez, L. Godeffroy, H. J. von Bardeleben, L. Fillaud, E. Maisonhaute, Y. Li, L.-M. Chamoreau and R. Lescouëzec, *J. Am. Chem. Soc.*, 2022, **144**, 10888.
- 42 A. Bleuzen, V. Escax, J.-P. Itié, P. Münsch and M. Verdaguer, *C. R. Chim.*, 2003, **6**, 343.
- 43 V. Escax, C. Cartier dit Moulin, V. Villain, G. Champion, J.-P. Itié, P. Münsch, M. Verdaguer and A. Bleuzen, *C. R. Chim.*, 2003, **6**, 1165.
- 44 P. Roy, M. Rouzières, Z. Qi and O. Chubar, *Infrared Phys. Technol.*, 2006, **49**, 139.
- 45 M. F. Faggin and M. A. Hines, *Rev. Sci. Instrum.*, 2004, **75**, 4547.
- 46 S. P. Davis, M. C. Abrams and J. J. W. Brault, *Fourier Transform Spectrometry*, Academic Press, San Diego, CA, 2001.

